Improving Tissue Segmentation of Human Brain MRI Through Pre-Processing by the Gegenbauer Reconstruction Method

Rick Archibald,[b] Kewei Chen,[c] Anne Gelb,[a] and Rosemary Renaut.[a]

[a] *Arizona State University, Department of Mathematics and Statistics, Tempe, Arizona 85287-1804.*

[b] *The Center for System Science and Engineering Research (SSERC), Arizona State University, Tempe, Arizona 85287-1804.*

[c] *Samaritan PET Center, Good Samaritan Regional Medical Center, 1111 E. McDowell Road, Phoenix, Arizona, 85006.*

Abstract

The Gegenbauer image reconstruction method, previously shown to improve the quality of magnetic resonance images, is utilized in this study as a segmentation pre-processing step. It is demonstrated that, for all simulated and real magnetic resonance images used in this study, the Gegenbauer reconstruction method improves the accuracy of segmentation. Although it is more desirable to use the k-space data for the Gegenbauer reconstruction method, only information acquired from MR images is necessary for the reconstruction, making the procedure completely self contained and viable for all human brain segmentation algorithms.

Key words: Segmentation, Brain Extraction, Edge Detection, Gegenbauer Reconstruction, Noise.

1 INTRODUCTION

Magnetic resonance imaging (MRI) is a noninvasive procedure that has proven to be an effective tool in the study of the human brain. The information that MRI provides has greatly increased knowledge of normal and diseased anatomy

for medical research, and is a critical component in diagnosis and treatment planning.

Image segmentation algorithms for the delineation of 3D anatomical structures, or tissue types, play an important role in numerous research and clinical studies, involving the visualization and quantitative analyzes of anatomical and functional cortical structures (Worth *et al.*, 1997; Dale *et al.*, 1999; Van Essen *et al.*, 1999; Joshi *et al.*, 1999). Guided neural surgery using segmented magnetic resonance images has grown in popularity in treating brain-related diseases such as epilepsy and stroke (Khoo *et al.*, 1997; Roux *et al.*, 1997; Le Bihan, 2000; Taylor, 1995). Functional visualization, in which a segmented brain can provide an anatomical framework, has emerged as a promising approach in neuroscience research and in neurosurgical planning owing to the advancement of brain function studies using functional MRI (fMRI) (Kwong *et al.*, 1992; Ogawa *et al.*, 1992; Liu *et al.*, 2000; Logothetis *et al.*, 2001) and Positron Emission Tomography (PET) (Chen *et al.*, 2001). The segmentation of brain images is also widely used in cortical surface mapping, volume measurement, tissue classification and differentiation, functional and morphological adaptation assessment, and characterization of neurological disorders such as multiple sclerosis, stroke, and Alzheimer's disease (Rusinek *et al.*, 1991; Suckling *et al.*, 1999; Le Goualher, 2000). Moreover, brain segmentation is also a required preliminary step for many other image-processing procedures, such as brain registration, warping (Lemieux, 1998; Ghanei *et al.*, 2000; Joshi *et al.*, 1997), and voxel-based morphometry (Ashburner and Friston, 2000). The fact that many applications depend on accurate brain segmentation has inspired much work for its improvement.

The focus of this study is to improve segmentation through the use of the Gegenbauer reconstruction method as a pre-processing step. The Gegenbauer reconstruction method is a high resolution method, introduced in (Gottlieb *et al.*, 1992), and established as an effective reconstruction method for magnetic resonance imaging in (Archibald and Gelb, 2002a). Using simulated brain phantom data (Brainweb, 2003) and data from real patients, this study shows that the Gegenbauer reconstruction method improves the quality of the MRI data and the subsequent brain tissue maps generated by SPM (SPM Website, 2003) segmentation algorithm.

2 METHODS

2.1 Segmentation Preprocessing Using the Gegenbauer Reconstruction Method

The Gegenbauer reconstruction method, introduced in (Gottlieb *et al.*, 1992), is a high resolution image reconstruction technique which is capable of reconstructing images with exponential accuracy, including the edges of structures in the image, without blurring features, hence mitigating a common problem associated with image filtering. Since the locations of the edges are needed to determine the regions of smoothness in which the images can be reconstructed (Gottlieb and Shu, 1997) , a critical first step in all high resolution reconstruction is edge detection. Edge detection is achieved by a combination of the edge detection procedure designed in (Gelb and Tadmor, 1999) and (Gelb and Tadmor, 2000), with the minimization procedure introduced in (Archibald and Gelb, 2002a). The edge detection and Gegenbauer reconstruction methods are briefly outlined in the appendix in sections 6.1 and 6.2. As described in these sections, the employment of the FFT algorithm for the both the edge detection and Gegenbauer reconstruction method ensures that the speed of computation is of the order of conventional FFT image reconstruction.

2.2 Windowed Reconstructed Data

Given the Fourier reconstruction of an image it is possible to determine the edges via the concentration method (Gelb and Tadmor, 1999). Once the edges are known, high resolution image reconstruction of the entire image is achieved by using the Gegenbauer reconstruction method in each smooth region. Typically the edge detection and Gegenbauer reconstruction procedures require knowledge of the original Fourier coefficients (or k-space data) which are imbedded (Liang and Lauterbur, 2000) in RF signal collected during a MR acquisition. However, often what is available to the researchers/physicians are the windowed (or filtered) Fourier reconstruction data, i.e. the conventional MRI data. Although less desirable, this still provides sufficient information for both the edge detection and Gegenbauer reconstruction procedures. Proofs of the previous statement are given in the appendix in order to demonstrate the broad application of the Gegenbauer reconstruction method to MR imaging segmentation. This study will only use windowed reconstructed data in order to demonstrate the effectiveness of the edge detection and Gegenbauer reconstruction procedures on conventional MRI data.

2.3 Segmentation

Segmentation is performed using the well known Statistical Parametric Mapping (SPM) program developed by the methodology group at the Wellcome Department of Cognitive Neurology (SPM Website, 2003). Statistical Parametric Mapping is publically available software used to test hypotheses about [neuro] imaging data from Single Photon Emission Computed Tomography (SPECT), PET and fMRI. Of particular interest to this study is the segmentation program bundled in this software. SPM segments spatially normalized images into gray matter (GM), white matter (WM), and cerebrospinal fluid (CSF), using a modified mixture model cluster analysis technique (Ashburner and Friston, 1997), and is extended to include a correction for image intensity nonuniformity (Ashburner and Friston, 2000) that arises from various sources in MR imaging.

The current version of SPM used in this study is SPM2b. The default settings were used in segmentation and brain extraction. This version, as compared to previous versions, has improved segmentation and brain extraction utilities, for which details are outlined on the SPM website (SPM Website, 2003). We note that other segmentation algorithms (Liang *et al.*, 1994; Schroeter *et al.*, 1998; Aizenberg *et al.*, 1998; Wu *et al.*, 1998) when used in conjunction with Gegenbauer reconstruction as a pre-processing step, including SPM99, produce similar results as those presented in this study (Archibald, 2002). Therefore we conclude that the accuracy of general segmentation is improved by using the Gegenbauer method as a pre-segmentation step.

3 EXPERIMENTAL METHODS

3.1 Data Acquisition: MNI Digital Brain Phantom

The effect of the Gegenbauer reconstruction method on the results of brain tissue segmentation was evaluated for simulated MRI scans (Brainweb, 2003) of a MNI digital brain phantom (Kwan *et al.*, 1996; Cocosco *et al.*, 1997; Collins *et al.*, 1998). Brainweb is maintained by the Brain Imaging Center at the Montreal Neurological Institute. The simulated MRI data was generated with noise levels of 5%, 7%, and 9%, with intensity non-uniformity (INU) of 20%, and 40%. Ten images were generated for each combination of noise and intensity non-uniformity for a total of sixty random images generated by Brainweb (Brainweb, 2003). Each generated image simulated a T1 weighted single channel MRI scan using the SFLASH (Spoiled FLASH) pulse sequence collected in the transverse direction. The parameters for each generated image

were as follows: TR, 18 ms; TE, 10 ms; flip angle, 30°; FOV, 256 mm $\times$ 256 mm; number of slices (contiguous), 256; slice thickness, 1 mm; in-slice resolution 1 mm $\times$ 1 mm.

3.2 Data Acquisition: Real Data

We used real MRI data from six consenting normal healthy subjects. Their MR data was acquired using a 1.5 T Signa system (General Electric, Milwaukee, WI) and T1 weighted, three-dimensional pulse sequence (radio-frequency-spoiled gradient recall acquisition in the steady state (SPGR), repetition time =33 msec, echo time = 5 msec, $\alpha = 30°$, number of excitations= 1, field of view= 24cm, imaging matrix= 256 $\times$ 192, slice thickness= 1.5mm, scan time= 13 : 36 min). The MR data set consisted of 124 contiguous horizontal slices with in-plane voxel dimension of 0.94 by 1.25mm.

3.3 Validation: MNI Digital Brain Phantom

The probability maps for gray matter (GM) and white matter (WM) for each MNI digital brain phantom that is generated by SPM segmentation are compared to the corresponding 'true' tissue probability map using the average absolute value norm over all voxels, where the norm is defined for an arbitrary image $A \in \mathbb{R}^{N_x} \times \mathbb{R}^{N_y} \times \mathbb{R}^{N_z}$ as

$$| A |= \frac{1}{N_x N_y N_z} \sum_{i_x}^{N_x} \sum_{i_y}^{N_y} \sum_{i_z}^{N_z} | a_{i_x,i_y,i_z} | . \tag{1}$$

An error measurement is calculated for a given segmented tissue probability map, P_S, and the Brainweb 'truth' tissue probability map P_T as

$$E(P_T, P_S) =| P_T - P_S | . \tag{2}$$

Note that in addition to tissue probability maps, Brainweb also provides a discrete tissue index map. Using the tissue index map as ground truth is most appropriate in the evaluation of binary segmentation. This study analyzes the probability maps generated by SPM, where it is appropriate to use Brainweb's tissue probability maps as ground truth.

The κ index (Dice coefficient) is a parameter that has frequently been reported in the literature (Collins *et al.*, 1999; Van Leemput *et al.*, 1999; Shattuck *et*

al., 2001) to evaluate the similarity of two images. Given two binary images, S_1 and S_2, the κ index is calculated as

$$\kappa(S_1, S_2) = \frac{2 \mid S_1 \cap S_2 \mid}{\mid S_1 \mid + \mid S_2 \mid}. \tag{3}$$

Since probability maps are not binary images, a threshold is applied in order to use the κ index as a method to compare the SPM segmented tissue maps to ground truth. For a given segmented tissue probability map, P_S, and the Brainweb 'truth' tissue probability map, P_T, two binary images that represent the body of the tissue are generated by setting each pixel, p, of both probability maps to a new threshold value, s_{tb}, as

$$s_{tb} = \begin{cases} 1, \text{ if } p \geq .95 \\ 0, \text{ else.} \end{cases} \tag{4}$$

For these two binary images the κ index (3) is calculated, which, in this case, measures how well the segmented tissue probability map approximates the body of the tissue.

Similarly for a given segmented tissue probability map, P_S, and the Brainweb 'truth' tissue probability map, P_T, two different binary images that represent the boundary or partial volume region are generated by setting each pixel, p, of both probability maps to a new threshold value, s_{pv}, as

$$s_{pv} = \begin{cases} 1, \text{ if } .05 \leq p < .95 \\ 0, \text{ else.} \end{cases} \tag{5}$$

The κ index (3) is calculated for these two binary images and in this case measures how well the segmented tissue probability map approximates the partial volume region of the tissue.

The thresholds defined above allow comparisons of the core and partial value regions of the gray/white tissue matter more specifically. Therefore, we refer to this method as the local measurement. Different thresholds, other than .95 and .05, have been applied yielding similar results.

3.4 Validation: Real Data

Since ground truth tissue maps are not available for real MR data, the quality of the SPM segmented tissue probability maps via Gegenbauer reconstruction pre-processing were assessed by visually inspecting the quality of the extracted brain cortical surface. The SPM brain extraction utility relies exclusively on segmented data to estimate the brain cortical surface. It is assumed in this study that visually apparent artifacts in brain extraction, that are reduced through the utilization of the Gegenbauer reconstruction method as a pre-segmentation step, demonstrate the ability of this method not only to improve brain extraction but also to improve segmentation. Thus the Gegenbauer reconstruction method as a pre-segmentation step is validated for real data in this study by analyzing visually apparent brain extraction artifacts.

4 RESULTS

4.1 Global Error Measurements

Table 1 displays the average tissue probability map error measurement (2) for each combination of noise and intensity non-uniformity for both gray matter and white matter tissue. Using the Gegenbauer reconstruction method as a segmentation pre-processing step reduces the error measurement for each combination of noise and intensity non-uniformity for both tissue types. As the level of noise increases, so does the average amount of error reduction between the original reconstruction and the Gegenbauer reconstruction. The segmentation improvement using Gegenbauer reconstruction is statistically significant for each noise level and inhomogenity level combination ($p < 0.05$ paired t-test). The p-values decreased with the level of noise, and are of the order 10^{-5} for the 9% noise level.

Depicted in figures 1 and 2 are gray matter and white matter segmented probability maps for the original and Gegenbauer image reconstruction of a particular randomly generated MNI digital brain phantom with 9% level of noise and 40% intensity non-uniformity. Visually it can be seen that there is a difference in the accuracy of the probability maps when Gegenbauer reconstruction is used as a segmentation pre-processing step.

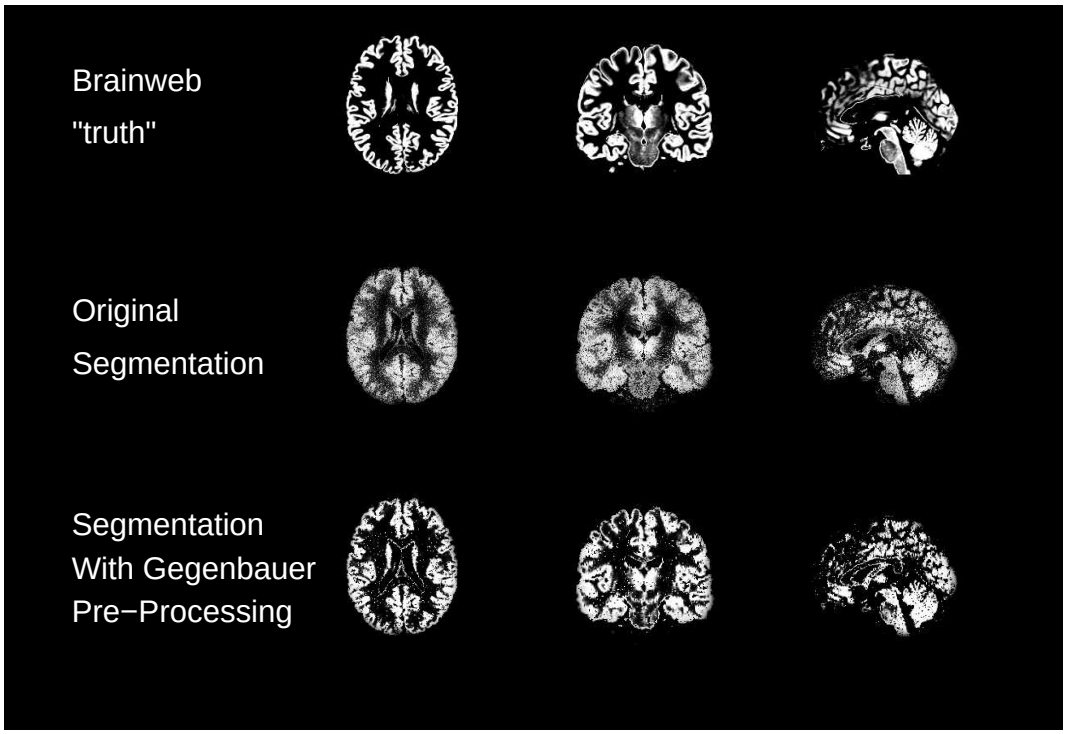

Fig. 1. Gray matter segmented probability maps for the original and Gegenbauer image reconstruction of a particular randomly generated MNI digital brain phantom with a 9% level of noise and 40% intensity non-uniformity.

Table 1
Tissue probability map error measurement (2) statistics for randomly generated MNI digital brain phantoms.

		Tissue			
		Gray Matter		White Matter	
Noise	INU	Original	Gegenbauer	Original	Gegenbauer
5%	20%	4.181 ± 0.009	3.302 ± 0.008	2.831 ± 0.008	2.023 ± 0.007
	40%	4.253 ± 0.011	3.391 ± 0.01	2.905 ± 0.011	2.054 ± 0.009
7%	20%	5.291 ± 0.017	3.649 ± 0.011	3.872 ± 0.013	2.352 ± 0.011
	40%	5.431 ± 0.024	3.711 ± 0.017	3.943 ± 0.018	2.372 ± 0.015
9%	20%	6.247 ± 0.021	4.118 ± 0.015	4.571 ± 0.018	2.548 ± 0.016
	40%	6.347 ± 0.032	4.131 ± 0.02	4.588 ± 0.019	2.579 ± 0.017

Comparison between each segmented probability map for original and Gegenbauer image reconstruction. All values are multiplied by $\times 10^{-2}$ and are written in the format of mean $\pm$ standard deviation.

4.2 Local Error Measurements

Table 2 displays the average tissue probability map error measurement (2) for each combination of noise and intensity non-uniformity for both gray matter

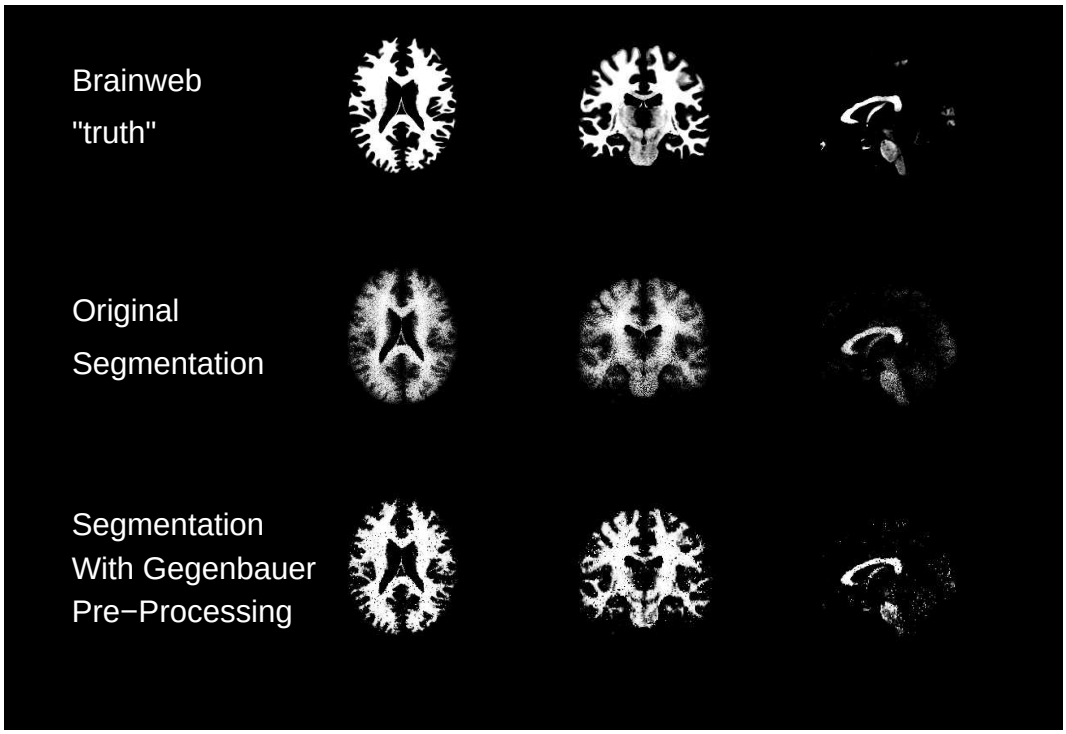

Fig. 2. White matter segmented probability maps for the original and Gegenbauer image reconstruction of a particular randomly generated MNI digital brain phantom with a 9% level of noise and 40% intensity non-uniformity.

and white matter tissue, where each probability map is restricted to its partial volume region, which is defined in (5). The results mirror table 1 in the sense that it is evident that by using the Gegenbauer reconstruction method as a segmentation pre-processing step, the error measurement is reduced for each combination of noise and intensity non-uniformity for both tissue types. Similarly, it is noticed that as the level of noise increases, the average amount of error reduction between the original reconstruction and the Gegenbauer reconstruction for the partial volume region grows. The segmentation improvement using Gegenbauer reconstruction is statistically significant for each noise level and inhomogenity level combination ($p < 0.01$ paired t-test). The p-values decreased with the level of noise, and are of the order 10^{-6} for the 9% noise level.

4.2.1 Similarity Measurement

In order to determine the κ index (3), binary images must be generated from each segmented probability map. The tissue body region (4) and partial volume region (5) are the generated binary images used to calculate the similarity coefficients. Depicted in figures 3 and 4 are gray matter and white matter partial volume region binary images of the segmented probability maps for the original and Gegenbauer image reconstruction of a particular randomly gen-

Table 2
Tissue probability map restricted to the partial volume region (5) error measurement (2) statistics for randomly generated MNI digital brain phantoms.

		Tissue			
		Gray Matter		White Matter	
Noise	INU	Original	Gegenbauer	Original	Gegenbauer
5%	20%	6.916 ± 0.011	5.893 ± 0.01	4.273 ± 0.008	2.745 ± 0.006
	40%	6.935 ± 0.012	5.897 ± 0.011	4.289 ± 0.011	2.753 ± 0.008
7%	20%	7.925 ± 0.016	5.985 ± 0.014	5.386 ± 0.012	2.849 ± 0.009
	40%	7.941 ± 0.024	5.991 ± 0.021	5.403 ± 0.018	2.869 ± 0.011
9%	20%	8.461 ± 0.023	6.191 ± 0.021	5.994 ± 0.017	2.994 ± 0.012
	40%	8.498 ± 0.03	6.201 ± 0.026	6.001 ± 0.018	3.011 ± 0.012

Comparison between each segmented probability map restricted to the partial volume region (5) for original and Gegenbauer image reconstruction. All values are multiplied by $\times 10^{-2}$ and are written in the format of mean $\pm$ standard deviation.

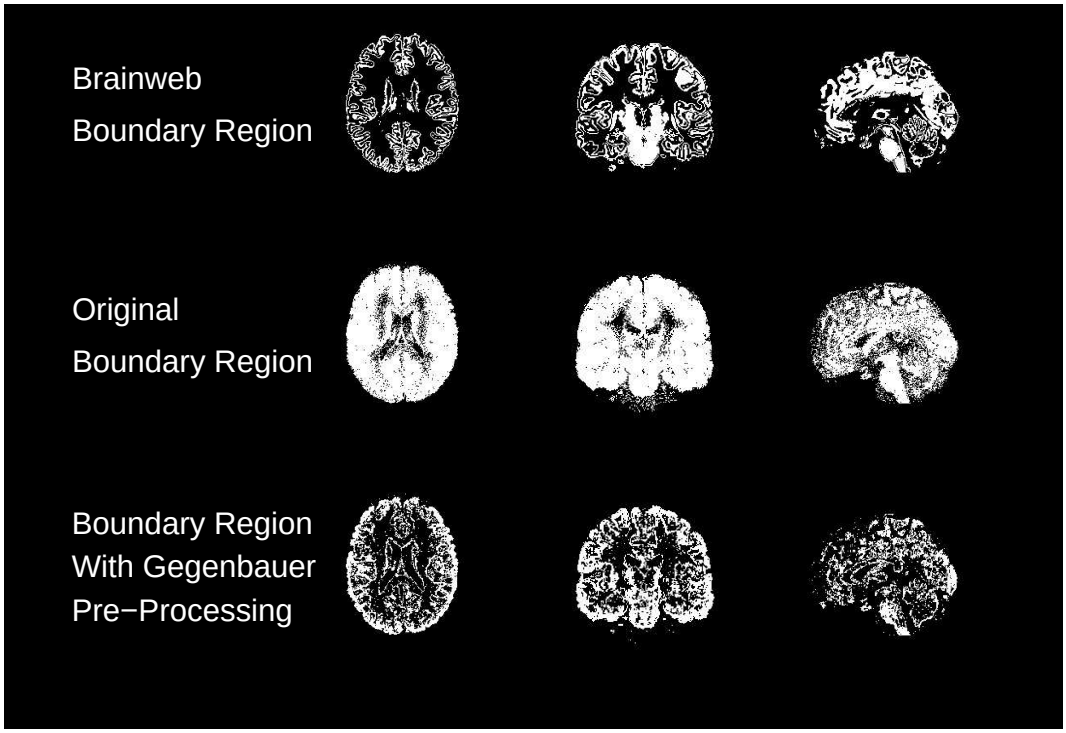

Fig. 3. Gray matter partial volume region binary image (5) generated from the segmented probability maps for the original and Gegenbauer image reconstruction of a particular randomly generated MNI digital brain phantom with a 9% level of noise and 40% intensity non-uniformity.

erated MNI digital brain phantom with a 9% level of noise and 40% intensity non-uniformity. There is a visual difference in the accuracy of the binary images of the probability maps when Gegenbauer reconstruction is used as a segmentation pre-processing step.

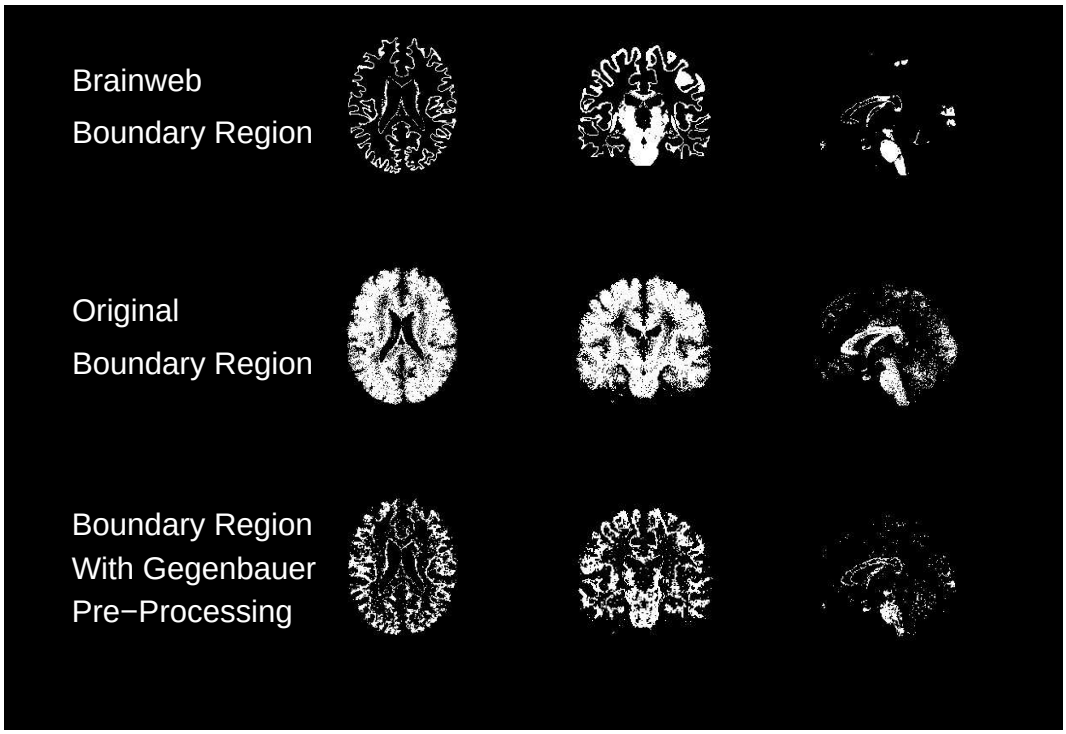

Fig. 4. White matter partial volume region binary image (5) generated from the segmented probability maps for the original and Gegenbauer image reconstruction of a particular randomly generated MNI digital brain phantom with a 9% level of noise and 40% intensity non-uniformity.

Table 3 displays the κ index for the partial volume region binary images generated from both gray matter and white matter segmented probability maps. Similarly, Table 4 displays the κ index for the tissue body region binary images generated from both gray matter and white matter segmented probability maps. Typically it is considered that $\kappa > .7$ indicates excellent agrement (Bartko, 1991) in binary images. It is noted that in many instances, particularly for white matter tissue, the use of Gegenbauer method as a pre-processing step improves the κ index beyond the critical value of .7, establishing that this pre-processing step has the ability to improve similarity between the segmented tissue probability maps and ground truth so that it is possible to conclude excellent agrement.

The κ index also has merit in the fact that it provides a value that can be used to compare the similarities between two measurement pairs (Zijdenbos *et al.*, 1994), which is the primary reason it is used in this study. It can been seen that there is significant improvement in the κ index coefficient for each tissue type and for all combinations of noise and intensity non-uniformity. Furthermore, the improvement of both similarity coefficient between the original and Gegenbauer reconstruction increases with the noise level. The improvement is even more dramatic for the similarity coefficients than for the error measurements. Using a Wilcoxon signed rank test, the significance level is $p < .01$ for

every combination of noise and intensity non-uniformity.

Table 3
κ index (3) statistics for tissue partial volume region binary images (5) generated from tissue probability maps of MNI digital brain phantoms.

		Tissue			
		Gray		White	
Noise	INU	Original	Gegenbauer	Original	Gegenbauer
5%	20%	0.484 ± 0.003	0.573 ± 0.003	0.551 ± 0.001	0.739 ± 0.001
	40%	0.481 ± 0.003	0.571 ± 0.003	0.543 ± 0.001	0.732 ± 0.001
7%	20%	0.276 ± 0.004	0.529 ± 0.004	0.482 ± 0.002	0.714 ± 0.002
	40%	0.271 ± 0.004	0.526 ± 0.004	0.474 ± 0.002	0.708 ± 0.002
9%	20%	0.104 ± 0.005	0.495 ± 0.005	0.427 ± 0.003	0.701 ± 0.003
	40%	0.101 ± 0.005	0.492 ± 0.005	0.417 ± 0.003	0.697 ± 0.003

Comparison between each tissue partial volume region binary images (5) generated from the segmented probability map for original and Gegenbauer image reconstruction. All values are written in the format of mean ± standard deviation.

Table 4
κ index (3) statistics for tissue body binary images (4) generated from tissue probability maps of MNI digital brain phantoms.

		Tissue			
		Gray		White	
Noise	INU	Original	Gegenbauer	Original	Gegenbauer
5%	20%	0.577 ± 0.002	0.698 ± 0.002	0.767 ± 0.001	0.896 ± 0.001
	40%	0.571 ± 0.002	0.695 ± 0.002	0.762 ± 0.001	0.895 ± 0.001
7%	20%	0.342 ± 0.003	0.689 ± 0.003	0.634 ± 0.001	0.863 ± 0.001
	40%	0.334 ± 0.003	0.681 ± 0.003	0.629 ± 0.002	0.861 ± 0.002
9%	20%	0.218 ± 0.004	0.638 ± 0.004	0.642 ± 0.002	0.829 ± 0.002
	40%	0.212 ± 0.004	0.635 ± 0.004	0.635 ± 0.002	0.823 ± 0.002

Comparison between each tissue body binary images (4) generated from the segmented probability map for original and Gegenbauer image reconstruction. All values are written in the format of mean ± standard deviation.

4.3 Real Data Evaluation

It has been reported that artifacts in brain extraction include non-brain tissue such as scalp in the final extracted image. In our study, we find that four out of six extractions presented this artifact, with severity varying from subject to subject. Figure 5 displays the results of SPM brain extraction of one particular subject, where the view on the right utilized the Gegenbauer reconstruction method as a pre-segmentation step. It is demonstrated that all

visually apparent artifacts are reduced by using the Gegenbauer method. Similar results were obtained with all subjects in this study with visually apparent artifacts. Additionally for all six subjects, no new visually apparent artifacts were generated.

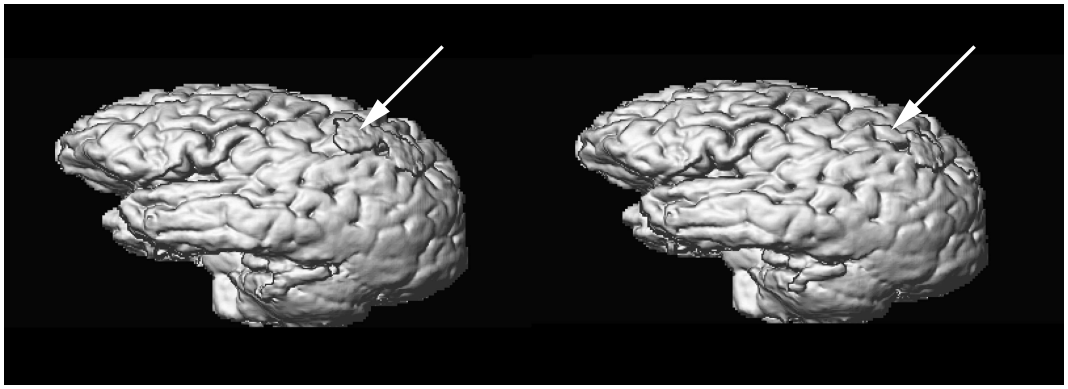

Fig. 5. SPM brain extraction of one particular subject, where the picture on the right used the Gegenbauer reconstruction method as a pre-segmentation step.

5 DISCUSSION AND CONCLUSION

As is demonstrated in section 4, the use of the Gegenbauer reconstruction method as a segmentation pre-processing step significantly improves the quality of the probability maps generated from SPM segmentation for both gray and white tissue. This improvement can be understood in terms of the differences in filtered Fourier reconstruction, which is the traditional method of reconstruction for MRI, and the Gegenbauer reconstruction.

The filtered Fourier method is the image reconstruction technique used for the real and simulated data in this study. Filters are often introduced to dampen the high frequency modes which reduce the effects of Gibbs ringing artifact and noise. Filtering is a violation of the data-consistency constraint, but is tolerated in order to reduce the Gibbs ringing artifact (Liang and Lauterbur, 2000) and suppress noise.

There is important information that is carried in the high frequency modes that pertain to finer features of the reconstructed image. The Gegenbauer reconstruction method, introduced in (Gottlieb *et al.*, 1992), does not violate the data consistency constraint and is capable of reconstructing piecewise smooth functions in smooth intervals with exponential accuracy up to the edges of the interval without blurring the features at the boundaries. This is reflected in section 4.2, in the improvement of both the tissue partial volume region and the tissue body region. The Gegenbauer reconstruction method's

ability to reconstruct sharp boundaries is suggestive of the minimization of visual artifacts in brain extraction in section 4.3.

Noise prevalent in MRI spectral data is an impediment to image reconstruction. This noise is difficult to quantify and can not be systematically removed. A preliminary investigation was conducted in (Archibald and Gelb, 2002b) to address the effects of noisy spectral data on the ability of the concentration method to locate edges and the Gegenbauer method to reconstruct images. As demonstrated throughout section 4, the application of the edge detection and high resolution reconstruction methods discussed in this paper not only recovers images with very high accuracy, but is also robust in the presence of noise, and additionally reduces the effects of noise.

Figure 6 depicts the method for implementing Gegenbauer reconstruction as a pre-segmentation step. In order not to violate the data-consistency constraint, k-space data should be used for both edge detection and Gegenbauer reconstruction prior to segmentation. Often it is the case that only reconstructed data is available, thus this study demonstrates the viability of using reconstructed data for edge detection and Gegenbauer reconstruction to improve the results of segmentation.

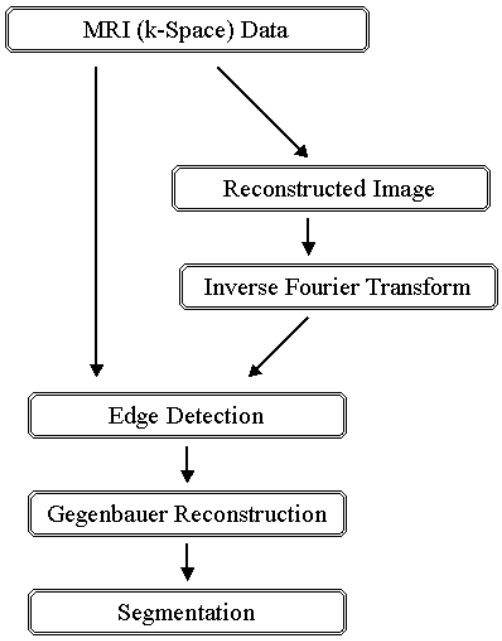

Fig. 6. Flow chart of the Gegenbauer reconstruction method as a segmentation pre-processing step.

This research opens new directions in the application of high resolution techniques in the field of MRI.

6 APPENDIX

Section 2.1 discuses the boundary detection and high resolution reconstruction method used in this paper, which are described in greater detail below in sections 6.1 and 6.2. Both the edge detection and reconstruction method require the knowledge of k-space data. Often, as is the case with this study, what is known are the windowed reconstructed data, and therefore it is proven in section 6.3 that using the windowed reconstructed data will only minimally effect the the results of the Gegenbauer reconstruction method. However we stress that knowledge of the unfiltered k-space data is preferable in order to satisfy the data-consistency constraint (Liang and Lauterbur, 2000).

6.1 Edge Detection

The concentration edge detection method is first described for one dimension. Define the jump function $[f](x)$ for a piecewise smooth function as $[f](x) = f(x+) - f(x-)$, where $f(x\pm)$ are the right and left side limits of the function at x, $f(x\pm) = lim_{x\to x\pm} f(x)$. Note that $[f](x)$ is zero away from a discontinuity, and is the value of the jump at a discontinuity.

It is shown in (Gelb and Tadmor, 1999) that the concentration method for detecting jump discontinuities is easily implemented in the discrete case as

$$T_N^\tau[f](x) := i\pi \sum_{k=-N}^{N} sgn(k)\tau\left(\frac{|k|}{N+\frac{1}{2}}\right)\tilde{f}_k e^{ik\pi x} \longrightarrow [f](x), \qquad \text{as } N \longrightarrow \infty. \tag{6}$$

Here $\tilde{f}_k$ are the discrete Fourier coefficients computed using the Fast Fourier Transform (FFT) algorithm from given discrete data $f(x_j)$, $x_j = -1 + \frac{j}{N}$, $j = 0, \ldots, 2N-1$, as

$$\tilde{f}_k = \frac{1}{2Nc_k} \sum_{j=0}^{2N-1} f(x_j) e^{-i\pi k x_j}, \qquad c_k = \begin{cases} 2, \text{ if } k = \pm N, \\ 1, \text{ otherwise,} \end{cases} \tag{7}$$

and $\tau(\xi)$ is determined in (Gelb and Tadmor, 1999) as

$$\tau(\xi) = \sigma(\xi)\frac{2\sin(\xi\pi)}{\xi\pi}, \tag{8}$$

where $\sigma(\xi)$ is a continuous concentration factor that satisfies

$$\frac{\sigma(\xi)}{\xi} \in C^2(0,1),$$

and normalized so that

$$\int_0^1 \frac{\sigma(\xi)}{\xi} d\xi = 1.$$

There are several examples of admissible concentration factors discussed in (Gelb and Tadmor, 1999). The exponential concentration factor,

$$\sigma(\xi) = c\xi e^{\frac{1}{\alpha\xi(\xi-1)}}, \tag{9}$$

where

$$c = \int_{\epsilon}^{1-\epsilon} exp\left(\frac{-1}{\alpha\eta(\eta-1)}\right) d\eta, \tag{10}$$

is particularly effective, as it takes full advantage of the spectral data by rapidly converging away from the discontinuities. The parameter α is freely chosen, with a typical value $\alpha = 6$. We note that when the data given are k-space data, the edge detection method (6) can be directly applied and easily calculated with the FFT algorithm.

In order to determine the exact intervals of smoothness, which is imperative for high resolution reconstruction, the concentration method (6) must be further enhanced to "pinpoint" the edges exactly. For this purpose, an edge enhancement procedure based on a separation of scales, has been constructed in (Gelb and Tadmor, 2000),

$$E_N(T_N^\tau[f](x)) = \begin{cases} T_N^\tau[f](x), \text{ if } |N^{q/2}(T_N^\tau[f](x))^q| > J_{crit}, \\ \\ 0, \qquad\qquad \text{if } |N^{q/2}(T_N^\tau[f](x))^q| < J_{crit}. \end{cases} \tag{11}$$

Here J_{crit} is an $\mathcal{O}(1)$ global threshold parameter signifying the minimal amplitude for the jump discontinuity not to be negligible. Since (6) actually locates the neighborhoods of the discontinuities, the exact jump locations are determined as the corresponding locations of the largest amplitudes $|E| > J_{crit}$ in each neighborhood of admissible jumps (i.e. where $|E| > J_{crit}$). Note that J_{crit} should be chosen to be consistent with the variation and scaling of the function. Experiments show that the parameter $q = 2$ is adequate for enhancement.

The nonlinear enhancement procedure (Gelb and Tadmor, 2000) works well when the discontinuities are located "far enough" from each other. (Experimentally the neighborhood of a discontinuity is approximately $5\Delta x$.) When the discontinuities are extremely close together, as is the case for MRI scans, where two neighboring pixels may contain discontinuities, a more refined procedure near the locations of the discontinuities must be employed. We adopt a minimization procedure (Archibald and Gelb, 2002a) given by

$$\min_{M,a_i,b_i} \max_x |T_N^\tau[h](x)| := \min_{M,a_i,b_i} \max_x |T_N^\tau[f](x) + \sum_{i=1}^{M} \frac{a_i}{2} T_N^\tau[g](x;b_i)|, \tag{12}$$

where

$$h(x) := f(x) + \sum_{i=1}^{M} \frac{a_i}{2} g(x;b_i) \tag{13}$$

and

$$g(x;b_i) = \begin{cases} x+1, \text{ if } -1 \le x \le b_i, \\ x-1, \text{ if } b_i < x \le 1. \end{cases} \tag{14}$$

Since $h(x)$ is a smooth function, $T_N^\tau[h](x) \longrightarrow 0$, and therefore the correct minimization of (12) yields the number of discontinuities, M, with the associated positions, b_i, and magnitudes, a_i, for $i = 1, \ldots, M$, of the function f.

The edge detection method and minimization process can be extended to detect the size and position of discontinuities of a multiple dimensional function by holding all but one dimension fixed and determining the edges as a function of the fixed coordinates. This three dimensional procedure is used for all images processed in this paper. The employment of the FFT algorithm for the boundary detection procedure ensures that the speed of computation is of the order of the three dimensional FFT.

6.2 Gegenbauer Reconstruction Method

The Gegenbauer reconstruction method was developed in (Gottlieb *et al.*, 1992) and extended in a litany of articles (consult Gottlieb and Shu (1997) for references). It is a powerful tool that recovers piecewise smooth functions with spectral accuracy up to the edges in each smooth interval, and can therefore be

used to completely eliminate the Gibbs ringing artifact without compromising high resolution at the edges.

Let us first introduce the Gegenbauer reconstruction method for a one dimensional piecewise smooth function $f(x)$. The Gegenbauer reconstruction method is performed on each smooth interval $[a, b] \subset [-1, 1]$. Specifically, define a local variable $\eta \in [-1, 1]$ such that $x(\eta) = \epsilon\eta + \delta$, where $\epsilon = \frac{b-a}{2}$ and $\delta = \frac{b+a}{2}$. The Gegenbauer reconstruction is then based on the Fourier approximation of $f(x)$ in $[a, b]$,

$$f_N(x(\eta)) = f_N(\epsilon\eta + \delta) = \sum_{k=-N}^{N} \tilde{f}_k e^{ik\pi(\epsilon\eta+\delta)}, \tag{15}$$

where $\tilde{f}_k$ is defined in (7), and is computed by

$$g_m^\lambda(x(\eta)) = \sum_{l=0}^{m} \tilde{g}_\epsilon^\lambda(l) C_l^\lambda(\eta), \tag{16}$$

where the Gegenbauer polynomial $C_n^\lambda(x)$ is an orthogonal polynomial of order n that satisfies

$$\int_{-1}^{1} (1-x^2)^{\lambda-\frac{1}{2}} C_k^\lambda(x) C_n^\lambda(x) dx = \begin{cases} h_n^\lambda, & k = n, \\ 0, & k \neq n, \end{cases} \tag{17}$$

where (for $\lambda \geq 0$)

$$h_n^\lambda = \frac{\sqrt{\pi} C_n^\lambda(1) \Gamma(\lambda + \frac{1}{2})}{\Gamma(\lambda)(n+\lambda)}, \tag{18}$$

with

$$C_n^\lambda(1) = \frac{\Gamma(n+2\lambda)}{n!\Gamma(2\lambda)}. \tag{19}$$

The approximate Gegenbauer coefficients,

$$\tilde{g}_\epsilon^\lambda(l) = \frac{1}{h_l^\lambda} \int_{-1}^{1} (1-\eta^2)^{\lambda-\frac{1}{2}} f_N(x(\eta)) C_l^\lambda(\eta) d\eta, \tag{20}$$

are computed by the FFT algorithm as

$$\tilde{g}_{\epsilon}^{\lambda}(l) = \sum_{k=-N}^{k=N} \bar{c}_k^{\lambda,l,\epsilon} e^{ik\pi\delta} \tilde{f}(k), \tag{21}$$

where

$$\bar{c}_k^{\lambda,l,\epsilon} = \begin{cases} 1, & \text{if } k = 0, \\ \Gamma(\lambda) i^l (l+\lambda) J_{l+\lambda}(\pi k \epsilon) \left(\frac{2}{\pi k \epsilon}\right)^{\lambda}, & \text{if } k \neq 0. \end{cases} \tag{22}$$

Here $J_{l+\lambda}(\pi k \epsilon)$ is the Bessel function. It is noted here that some smooth intervals may consist of too few points to construct an approximation. The Gegenbauer reconstruction requires at least a theoretical minimum of π points to form an approximation (Gottlieb and Orszag, 1977). Therefore, in these intervals, the values at each grid point are assumed constant and equivalent to the values determined at the edges by the edge detection method (Archibald and Gelb, 2002a).

The parameters m and λ depend upon the number of points, N_I, in the subinterval that is reconstructed. A specific requirement is that $m \leq N_I$. Recent work demonstrates how the parameters m and λ can be optimized for a particular subdomain (Gelb, In Press). For simplicity, we choose the parameters such that $\lambda = m$ with

$$m = \max\left\{1, \min\left\{m_{max}, \left[\frac{N_I}{4}\right]\right\}\right\}, \tag{23}$$

where $\left[\frac{N_I}{4}\right]$ is the nearest integer to $\frac{N_I}{4}$, and $m_{max} = 12$.

The Gegenbauer reconstruction method can be directly extended to multiple dimensions by performing reconstruction in smooth regions. The reconstruction will have exponential accuracy up to the edges of each smooth region. Three dimensional Gegenbauer reconstruction is used for all the images processed in this paper. The computational cost of the Gegenbauer reconstruction method is of the order of the three dimensional FFT. We note that different values can be chosen for λ and m in each dimension, which can be optimized by the size of the particular subdomain as demonstrated in (Gelb, In Press). However, for simplicity we adopt the parameters for each dimension according to (23). Convergence analysis of the Gegenbauer reconstruction method for the one dimensional case is provided in the next section.

One factor contributing to the Gibbs ringing artifact for piecewise smooth functions is the slow decay rate of the Fourier expansion coefficients (Gottlieb and Orszag, 1977). A window (or filter) increases the rate of decay by attenuating the higher order coefficients which in turn controls the effects of the Gibbs oscillations. The windowed discrete Fourier reconstruction is computed as

$$f_N^w(x) = \sum_{k=-N}^{N} w_k \tilde{f}_k e^{i\pi kx}, \tag{24}$$

where $w_k = w\left(\frac{|k|}{N}\right)$ is a window function. Given reconstructed data on equally spaced points the inverse transform will result in the spectral data

$$\tilde{f}_k^w = w_k \tilde{f}_k, \tag{25}$$

where w is the widow function used in reconstruction.

An edge detection procedure designed in (Gelb and Tadmor, 1999) and (Gelb and Tadmor, 2000), and briefly outlined in section 6.1, uses Fourier coefficients to determine boundaries. In this study, the k-space data is not available but rather the windowed k-space data are known (25). Theorem 6.1 proves that the information required for high resolution reconstruction, namely the position of edges, is preserved if windowed k-space data are used in the edge detection procedure provided that the window function satisfies two basic requirements. The first requirement is that the window function, w, is

$$w(\xi) \in C^2(0,1).$$

This is the case with all commonly used widowed functions used to eliminate the Gibbs ringing artifact (Gottlieb and Shu, 1997). The second requirement is that

$$\int_0^1 \frac{w(\xi)\sigma(\xi)}{\xi} d\xi \neq 0,$$

where σ is the concentration factor used in the edge detection method. The flexibility in the choice of the concentration factor, allows admissible window functions. In this paper the window function used by Brainweb is a sinc function (Kwan *et al.*, 1999), and we use a exponential concentration factor (9) in edge detection, which together satisfy both requirements.

Theorem 6.1 *Using spectral data (25) in the concentration method (6) preserves the positions of the jump discontinuities, provided that*

$$C_w := \int_0^1 \frac{w(\xi)\sigma(\xi)}{\xi} d\xi \neq 0, \tag{26}$$

and

$$w(\xi) \in C^2(0,1) \tag{27}$$

Proof.

Using the spectral data (25) the concentration method (6) will become

$$\begin{aligned} T_N^{\tau,w}[f](x) &:= i\pi \sum_{k=-N}^{N} sgn(k)\tau\left(\frac{|k|}{N+\frac{1}{2}}\right)\tilde{f}_k^w e^{ik\pi x} \\ &= i\pi \sum_{k=-N}^{N} sgn(k) w_k \tau\left(\frac{|k|}{N+\frac{1}{2}}\right)\tilde{f}_k e^{ik\pi x}. \end{aligned} \tag{28}$$

Define the function

$$\tau_w(\xi) = \frac{w(\xi)\tau(\xi)}{C_w}, \tag{29}$$

where C_w is defined in (26). Since $w \in C^2(0,1)$ and τ is a concentration factor,

$$\frac{w(\xi)\tau(\xi)}{C_w \xi} \in C^2(0,1),$$

and

$$\int_0^1 \frac{w(\xi)\sigma(\xi)}{C_w \xi} d\xi = \frac{1}{C_w}\int_0^1 \frac{w(\xi)\sigma(\xi)}{\xi} d\xi = 1. \tag{30}$$

Thus τ_w is a concentration factor. Hence

$$\frac{i\pi}{C_w}\sum_{k=-N}^{N} sgn(k) w_k \tau\left(\frac{|k|}{N+\frac{1}{2}}\right)\tilde{f}_k e^{ik\pi x} \longrightarrow [f](x). \tag{31}$$

and

$$T_N^{\tau,w}[f](x) \longrightarrow C_w[f](x) \tag{32}$$

□

Thus it is possible to determine the position of the discontinuities. The size of the jumps will be off by a factor of C_w, but is acceptable since only the positions of the jumps are necessary in Gegenbauer reconstruction.

As shown in (Gottlieb *et al.*, 1992), if $f(x)$ is an arbitrary L_2-function on $[-1,1]$, then the error in the max norm

$$\begin{aligned}\max_{-1\le x\le 1}\Big|f(x)-\sum_{l=0}^{m}\tilde{g}^{\lambda}(l)C_l^{\lambda}(x)\Big| &\le \max_{-1\le x\le 1}\Big|f(x)-\sum_{l=0}^{m}\hat{f}^{\lambda}(l)C_l^{\lambda}(x)\Big| \\ &\quad+\max_{-1\le x\le 1}\Big|\sum_{l=0}^{m}\hat{f}^{\lambda}(l)C_l^{\lambda}(x)-\sum_{l=0}^{m}\tilde{g}^{\lambda}(l)C_l^{\lambda}(x)\Big| \\ &\equiv RE(\lambda,m)+TE(\lambda,m,N), \end{aligned} \tag{33}$$

is exponentially convergent for $\lambda = m = \beta N$, where $\beta < \frac{2}{27}\pi e$. The proof provided in (Gottlieb *et al.*, 1992) shows that both the regularization error (RE) and the truncation error (TE) are exponentially convergent. If it is assumed that what is known is the windowed reconstruction (24), then the error in the max norm becomes

$$\begin{aligned}\max_{-1\le x\le 1}\Big|f(x)-\sum_{l=0}^{m}\tilde{g}^{\lambda,w}(l)C_l^{\lambda}(x)\Big| \quad\le\quad &\max_{-1\le x\le 1}\Big|f(x)-\sum_{l=0}^{m}\hat{f}^{\lambda}(l)C_l^{\lambda}(x)\Big| + \\ &\max_{-1\le x\le 1}\Big|\sum_{l=0}^{m}\hat{f}^{\lambda}(l)C_l^{\lambda}(x)-\sum_{l=0}^{m}\tilde{g}^{\lambda,w}(l)C_l^{\lambda}(x)\Big|, \end{aligned} \tag{34}$$

where

$$\tilde{g}^{\lambda,w}(l) = \frac{1}{h_l^{\lambda}}\int_{-1}^{1}(1-x^2)^{\lambda-\frac{1}{2}}f_N^{w}(x)C_l^{\lambda}(x)dx. \tag{35}$$

If the error in (34) remains exponentially convergent, then the Gegenbauer reconstruction method utilizing the coefficients (35) generated from the windowed Fourier reconstruction will still yield high accuracy.

The following theorem is a slight modification of the theorem in (Gottlieb *et al.*, 1992) that proves the exponential convergence of the truncation error in (34). Specifically all of the original arguments for the exponential convergence proof are the same.

Theorem 6.2 *If $f(x)$ is an L_2-function on $[-1,1]$, then there exists a constant A which is independent of λ, m and N, such that the truncation error defined as*

$$TE(\lambda, m, N) \equiv \max_{-1\le x\le 1}\left|\sum_{l=0}^{m}\Big(\hat{f}^{\lambda}(l)-\tilde{g}^{\lambda,w}(l)\Big)C_l^{\lambda}(x)\right|, \tag{36}$$

satisfies the following estimate:

$$TE(\lambda, m, N) \le A\frac{(m+\lambda)\Gamma(m+2\lambda)\Gamma(\lambda)}{(m-1)!\Gamma(2\lambda)}\left(\frac{2}{\pi N}\right)^{\lambda-1}, \tag{37}$$

where w is a window (or filter) function.

Proof.

Before we prove the theorem for an arbitrary L_2-function on $[-1,1]$, consider the special function $f(x)=e^{in\pi x}$ with $|n|\ge N$. For this special case $f_N^w(x)=0$ and we obtain

$$\Big(\hat{f}^{\lambda}(l)-\tilde{g}^{\lambda,w}(l)\Big)C_l^{\lambda}(x)=\frac{C_l^{\lambda}(x)}{h_l^{\lambda}}\int_{-1}^{1}(1-x^2)^{\lambda-\frac{1}{2}}e^{in\pi x}C_l^{\lambda}(x)dx. \tag{38}$$

In (Bateman (1953); p.213) there is an explicit expression for (38) given by

$$\frac{1}{h_l^{\lambda}}\int_{-1}^{1}(1-x^2)^{\lambda-\frac{1}{2}}e^{in\pi x}C_l^{\lambda}(x)dx=\Gamma(\lambda)\left(\frac{2}{\pi n}\right)^{\lambda}i^l(l+\lambda)J_{l+\lambda}(\pi n). \tag{39}$$

Here $J_\nu(x)$ is the Bessel function. Since $|J_\nu(x)|\le 1$ for all x and $\nu\ge 0$ (Abramowitz and Stegun (1970); p.362), we have, for $0\le l\le m$,

$$\begin{aligned}\Big(\hat{f}^{\lambda}(l)-\tilde{g}^{\lambda,w}(l)\Big)C_l^{\lambda}(x) &\le C_l^{\lambda}(1)\Gamma(\lambda)\left(\frac{2}{\pi|n|}\right)^{\lambda}i^l(l+\lambda)\\ &=\frac{(l+\lambda)\Gamma(l+2\lambda)\Gamma(\lambda)}{l!\Gamma(2\lambda)}\left(\frac{2}{\pi|n|}\right)^{\lambda}\\ &=\frac{(m+\lambda)\Gamma(m+2\lambda)\Gamma(\lambda)}{m!\Gamma(2\lambda)}\left(\frac{2}{\pi|n|}\right)^{\lambda},\end{aligned} \tag{40}$$

where in the second step we used the formula

$$C_l^{\lambda}(1)=\frac{\Gamma(l+2\lambda)}{l!\Gamma(2\lambda)}, \lambda\ge 0, \tag{41}$$

and in the last step we used the fact that $(l+\lambda)\Gamma(l+2\lambda)/l!$ is a increasing function of l.

We now return to the general function $f(x)$, which by (Gottlieb and Shu, 1997) satisfies

$$f(x) - f_N^w(x) = \sum_{|n|>N} w_n \tilde{f}_n e^{i\pi n x}. \tag{42}$$

Since w is a filter function it is uniformly bounded with

$$|w_n| \leq 1. \tag{43}$$

Also since $f(x)$ is an L_2-function, it's Fourier coefficients $\tilde{f}_n$ are uniformly bounded. Hence

$$|w_n \tilde{f}_n| \leq |\tilde{f}_n| \leq A. \tag{44}$$

Therefore, using the result for the special case $e^{in\pi x}$ in (40) yields

$$\begin{aligned}\Big(\hat{f}^\lambda(l) - \tilde{g}^{\lambda,w}(l)\Big) C_l^\lambda(x) &\leq A \frac{(m+\lambda)\Gamma(m+2\lambda)\Gamma(\lambda)}{m!\Gamma(2\lambda)} \sum_{|n|>N} \left(\frac{2}{\pi|n|}\right)^\lambda \\ &= \tilde{A} \frac{(m+\lambda)\Gamma(m+2\lambda)\Gamma(\lambda)}{m!\Gamma(2\lambda)} \left(\frac{2}{\pi N}\right)^{\lambda-1},\end{aligned} \tag{45}$$

for all $0 \leq l \leq m$.

We can now estimate the truncation error (36) by

$$\begin{aligned}TE(\lambda, m, N) &\leq m \max_{0 leq l \leq m} \max_{-1 \leq x \leq 1} \Big(\hat{f}^\lambda(l) - \tilde{g}^{\lambda,w}(l)\Big) C_l^\lambda(x) \\ &\leq m \max_{0 leq l \leq m} \Big|\Big(\hat{f}^\lambda(l) - \tilde{g}^{\lambda,w}(l)\Big)\Big| C_l^\lambda(1) \\ &\leq A \frac{(m+\lambda)\Gamma(m+2\lambda)\Gamma(\lambda)}{(m-1)!\Gamma(2\lambda)} \left(\frac{2}{\pi N}\right)^{\lambda-1},\end{aligned} \tag{46}$$

where in the second step we used the fact that $|C_l^\lambda(x)| \leq C_l^\lambda(1)$ for all $-1 \leq x \leq 1$ (Bateman (1953); p.206), and in the third step we used (45).

□

The regularization error, $RE(m, \lambda)$ remains unchanged and proof of its exponential convergence can be found in (Gottlieb and Shu, 1997)

ACKNOWLEDGMENTS

The authors of this work were supported in part by the Arizona Center for Alzheimer's Disease Research (R. Archibald, K. Chen, A. Gelb, and R. Renaut), the Center for System Science and Engineering Research at Arizona State University (R. Archibald and A. Gelb), the Department of Mathematics and Statistics at Arizona State University (R. Archibald, K. Chen, A. Gelb, and R. Renaut), the John von Neumann visiting Professorship of the Zentrum Mathematik, Technische Universitaet Muenchen (R. Renaut), NSF grant No. DMS 9977234 (R. Renaut), and NSF grant No. DMS 01-07428 (A. Gelb).

References

Abramowitz, M. and Stegun, I.A. 1970. *Handbook of mathematical functions.* Dover, New York.

Aizenberg, I.N., Aizenberg, N.N., Gotko, E.S., and Sochka, V.A. 1998. Medical image processing using neural networks based on multi-values and universal binary neurons. SPIE Conference on image processing, San Diego, California.

Archibald, R. 2002. *Boundary detection and reconstruction in magnetic resonance imaging.* Thesis, Arizona State University.

Archibald, R. and Gelb, A. 2002. A method to reduce the Gibbs ringing artifact in MRI scans while keeping tissue boundary integrity. *IEEE Transactions of Medical Imaging*, **21**, 305-319.

Archibald, R. and Gelb, A. 2002. Reducing the effects of noise in boundary detection. *Journal of Scientific Computing*, **17**, 167-180.

Ashburner, J., and Friston, K.J. 1997. Multimodal image coregistration and partitioning–A unified framework. *NeuroImage*, **6**, 209-217.

Ashburner, J., and Friston, K.J. 2000. Voxel-based morphometry–The methods. *NeuroImage*, **11**, 805-812.

Bartko, J.J. 1991. Measurement and reliability: statistical thinking considerations. *Schizophrenia Bullet.*, **17**, 483-489.

Bateman, H. 1953. *Higher transcendental functions, Vol.2.* McGraw-Hill, New York.

Chen, J.L.,Gunn, S.R., Nixon, M.S. and Gunn, R.N. 2001. Markov random field models for segmentation of PET images. *Proceedings Information Processing in Medical Imaging*, **2082**, 468-474.

Cocosco, C.A., Kollokian, V. Kwan, R.K.-S., and Evans, A.C. 1997. BrainWeb: online interface to a 3D MRI simulated brain database. *NeuroImage*, **5**(4), part 2/4, S425.

Collins, D.L., Zijdenbos, A.P., Baaré, W.F., and Evans, A.C. 1999. ANIMAL + INSECT: Improved cortical structure segmentation. In *Lecture Notes in*

Computer Science, Vol. 1613, Proceedings of the 16th International Conference on Information Processing in Medical Imageing (A. Kuba, M. Sámal, and A. Todd-Pokropek, Eds), 463-468. Springer-Verlag. Berlin/Heidelberg.

Collins, D.L., Zijdenbos, A.P., Kollokian, V., Sled, J.G., Kabani, N.J., Holmes, C.J., and Evans, A.C. 1998. Design and construction of a realistic digital brain phantom. *IEEE Transactions on Medical Imaging*, **17**(3), 463-468.

Dale, A.M, Fischi, B., and Sereno, M.I. 1999. Cortical surface-based analysis. I. Segmenation and surface reconstruction. *NeuroImage*, **9**, 179-194.

Gelb, A. In Press. Parameter optimization and reduction of round off error for the Gegenbauer reconstruction method. Submitted to *Journal of Scientific Computing*.

Gelb, A. and Tadmor, E. 1999. Detection of edges in spectral data. *Applied and computational harmonic analysis*, **7**, 101-135.

Gelb, A. and Tadmor, E. 2000. Detection of edges in spectral data II: nonlinear enhancement. *SIAM J. Numer. Anal.*, **38**, 1389-1408.

Gelb, A. and Tadmor, E. 2000. Spectral reconstruction of piecewise smooth functions from their discrete data. *Mathematical Modelling and Numerical Analysis*.

Ghanei, A., Soltanian-Zadeh, H., Jacobs, M.A., and Patel, S. 2000. Boundary-based warping of brain MR images. *J. Magn. Reson. Imaging*, **12**, 417-429.

Gottlieb, D., Shu, C.W., Solomonoff, A. and Vandeven, H. 1992. On the Gibbs phenomenon I: recovering exponential accuracy from the Fourier partial sum of a nonperiodic analytic function. *J. of Comp. and appl. math.*, **43**, 81-98.

Gottlieb, D. and Orszag, S. 1977. *Numerical analysis of spectral methods: theory and applications*. SIAM, Philadelphia.

Gottlieb, D., and Shu, C.W. 1997. On the Gibbs phenomenon and its resolution.*SIAM Review*, **39**, 644-668.

Joshi, M., Cui, J., Doolittle, K., Joshi, S., Van Essen, D., Wang, L., and Miller, M.I. 1999. Brain segmentation and the generation of cortical surfaces. *NeuroImage*, **9**, 109-127.

Joshi, S., Miller, M., and Grenander, U. 1997. On the geometry and shape of brain sub-maifolds. *Int.J.Patt.Rec.Art.Intel.*, **11**, 1317-1343.

Khoo, V.S., Dearnaley, D.P., Finnigan, D.J., Padhani, A., Tanner, S.F., and Leach, M.O. 1997. Magnetic resonance imaging: consideration and applications in radiotheraphy treatment planning. *Radiother.Oncol.*, **42**, 1-15.

Kwan, R. K-S., Evans, A.C., and Pike, G.B. 1996. An extensible MRI simulator for post-processing evaluation. In *Lexture Notes in Computer Science.*, **1131**, 135-140. Springer-Verlag/Berlin.

Kwan, R.K-S., Evans, A.C., and Pike, G.B. 1999. MRI Simulation-based evaluation of image-processing and classification methods. *IEEE Transactions of Medical Imaging*, **18**, 1085-1097.

Kwong, K.K., Belliveau, J.W., Chesler, D.A., Goldberg, I.E., Weisskoff, R.M., Poncelet, B.P., Kennedy, D.N., Hoppel, B.E., Cohen, M.S., Turner, R., *et al.* Dynamic magnetic resonance imaging of human brain activity during primary sensory stimulation. *Proc. Natl. Acad. Sci. USA*, **89**, 5675-5679.

Le Bihan, D. 2000. What to expect from MRI in the investigation of the central nercous system? *C. R. Acad. Sci Ser. III*, **323**, 341-350.

Le Goualher, G., Argenti, A.M., Duyme, M., Baaré, W.F., Hulshoff Pol, H.E., Boomsma, D.I, Zouaoui, A., Barillot, C., and Evans, A.C. 2000. Statistical sulcal shape comparisons: Application to the detection of genetic encoding of the central sulcus shape. *NeuroImage*, **11**, 564-574.

Lemieux, L., Wieshmann, U.C., Moran, N.F., Fish, D.R., and Shorvon, S.D. 1998. The detection and significance of subtle changes in mixed-signal brain lesions by serial MRI scan matching and spatial normalization. *Med. Imaging Anal.*, **2**, 227-242.

Liang, Z. and Lauterbur, P. 2000. *Principles of magnetic resonance imaging, a signal processing perspective*. IEEE Press.

Liang, Z., MacFall, J.R., and Harrington, D.P. 1994. Parameter estimation and tissue segmentation for multispectral MR images. *IEEE T.Med.Imag.*, **13**, 441-449.

Lui, J.Z., Dai, T.H., Elster, T.H., Sahgal, V., Brown, R.W., and Yue, G.H. 2000. Simultaneous measurement of human joint force, surface electromyograms, and functional MRI-measured brain activation. *J. Neurosci. Methods*, **101**, 49-57.

Logothetis, N.K, Pauls, J., Augath, M., Trinath, T., and Oeltermann, A. 2001. Neurophysiological investigation of the basis of the fMRI signal. *Nature*, **412**, 150-157.

McConnell Brain Imaging Centre Montréal Neurological Institute MRI Simulator. <http://www.bic.mni.mcgill.ca/brainweb/>(10Jan. 2003).

Ogawa, S., Tank, D.W., Menon, R., Ellermann, J.M., Kim, S.G., Merkle, H., and Ugurbil, K. 1992. Intrinsic signal changes accompanying sensory stimulation: Functional brain mapping with magnetic resonance imaging. *Proc. Natl. Acad. Sci. USA*, **89**, 5951-5955.

Roux, F.E., Ranjeva, J.P., Boulanouar, K., Manelfe, C., Sabatier, J., Tremoulet, M., and Berry, I. 1997. Motor functional MRI for presurgical evaluation of cerebral tumors. *Stereotact. Funct. Neurosurg.*, **68**, 106-111.

Rusinek, H., De Leon, M.J., George, A.E, Stylopouoplos, L.A., Chandra, R., Smith, G., Rand, T., Mourino, M., and Kowalski, H. 1991. Alzheimer disease: Measuring loss of cerebral gray matter with MR imaging. *Radiology*, **178**, 109-114.

Schroeter, P., Vesin, J., Langenberger, T., and Meuli, R. 1998. Robust Parameter Estimation of Intensity Distributions for Brain Magnetic Resonance Images. *IEEE Transactions on medical imaging*, **17**(2), 154-165.

Shattuck, D.W., Sandor-Leahy, R.S., Schaper, K.A., Rottenberg, D.A., and Leahy, R.M. 2001. Magnetic resonance image tissue classification using a partial volume model. *NeuroImage*, **13**, 856-876.

Statistical Parametric Mapping. Wellcome Department of Cognitive Neurology <http://www.fil.ion.ucl.ac.uk/spm/>(12Jan. 2003).

Suckling, J., Sigmundsson, T., Greenwood, K., and Bullmore, E.T. 1999. A modified fuzzy clustering algorithm for operator independent brain tissue

classification of dual echo MR images. *Magn. Reson. Imaging*, **17**, 1065-1076.

Taylor, P. 1995. Invited Review: Computer aids for decision-making in diagnostic radiology- a literature review. *Brit.J.Radiol.*, **68**, 945-957.

Van Essen, D.C., Drury, H.A., and Anderson, C.H. 1999. An automated method for reconstructing complex surfaces, including the cerebral cortex. *Soc. Neurosci. Abstr.*, **25**.

Van Leemput, K., Maes, F., Vandermeulen, D., and Suetens, P. 1999. Automated model-based tissue classification of MR images of the brain. *IEEE Transactions of Medical Imaging*, **18**, 897-908.

Worth, A.J., Makris, N., Caviness, V.S., and Kennedy, D.N. 1997. Neuro-anatomical segmentation in MRI: technological objectives, *Int.J.Patt.Rec.Art.Intel.*, **111**, 1161-1187.

Wu, K., Schreiner, S., Mittelstadt, B., and Witherspoon, L. 1998. Image segmentation by gradient statistics. SPIE Conference on image processing, San Diego, California.

Zijdenbos, A.P., Dawant, B.M., Margolin, A.M., and Palmer, A.C. 1994. Morphometric analysis of white matter lesions in MR images: method and validation. *IEEE Transactions of Medical Imaging*, **13**, 716-724.